Passive Intermodulation in Distributed Circuits with Cascaded Discrete Nonlinearities

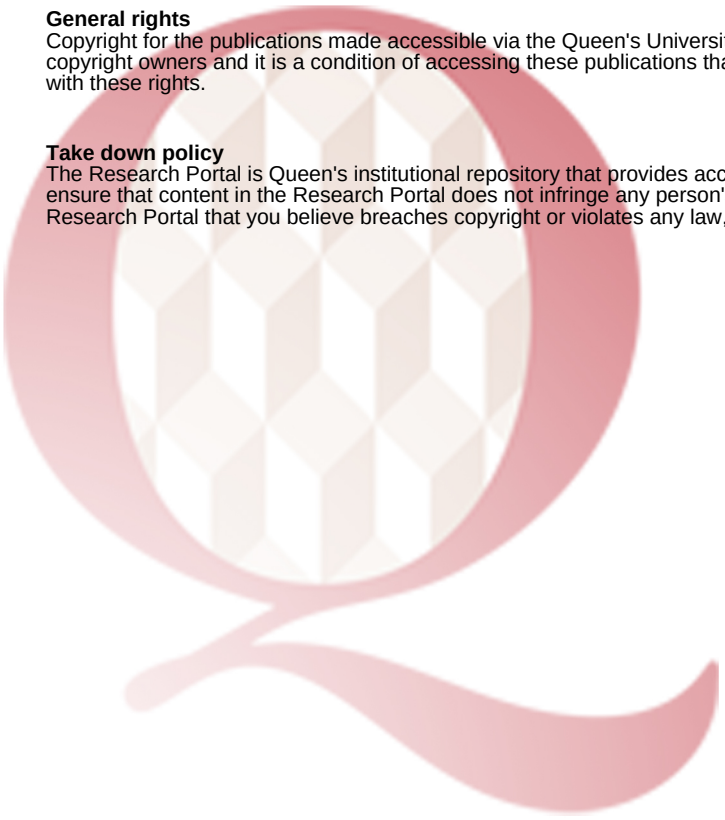

Passive Intermodulation in Distributed Circuits with Cascaded Discrete Nonlinearities

Dmitry S. Kozlov, Alexey P. Shitvov and Alexander G. Schuchinsky
Institute of Electronics, Communications and Information Technology (ECIT)
Queen's University Belfast
Queen's Road, Queen's Island, Belfast BT3 9DT, UK
d.kozlov@qub.ac.uk, a.shitvov@qub.ac.uk, a.schuchinsky@qub.ac.uk

***Abstract*—The principle aspects of passive intermodulation (PIM) characterisation in distributed printed circuits with cascaded lumped nonlinearities are presented. Mechanisms of PIM generations have been investigated experimentally and modelled using the formalism of X-parameters. The devised equivalent circuit models are applied to the analysis of microstrip lines with distributed and cascaded lumped sources of nonlinearity. The dynamic measurements have revealed that PIM generation rates in straight and meandered microstrip lines differ and significantly deviate from those expected for the respective discrete sources of nonlinearity. The obtained results indicate that multiple physical sources of nonlinearity contribute to PIM generation in printed circuits. Finally, it is demonstrated that the electrical discontinuities can have significant effect on the overall PIM response of the distributed passive circuits and cause PIM product leakage and parasitic coupling between isolated circuit elements.**

Keywords—intermodulation distortion; passive intermodulation (PIM); distributed nonlinearity; X-parameters, interference

I. INTRODUCTION

Intermodulation (IM) is conventionally defined as a phenomenon characterised by appearance of additional spectral components in the output spectrum of a multi-carrier system, which are not present in the original input signal [1]. Passive intermodulation (PIM) caused by weak nonlinearities may significantly distort signals and severely degrade the receiver sensitivity, ultimately resulting in dramatic reduction of data throughputs in wireless communication systems.

The signal integrity specifications in the base stations for mobile and space communications impose very stringent requirements to the PIM performance of RF front-end passive devices such as multiband antenna arrays, beamforming networks, phase shifters and filters. Majority of these devices are designed without preliminary assessment of their PIM performance which is later measured experimentally in a basic two-tone CW verification tests. However, such a procedure often leads to multiple design iterations to meet the required PIM specifications. Nor does it allow for location of the PIM sources and characterisation of the nonlinearity. Therefore, it is of high importance to incorporate the PIM analysis into the antenna and whole RF front-end design process and develop reliable predictive models of PIM generation.

PIM generation in antennas and passive RF components, such as connectors, coaxial cables, filters, duplexers and printed circuit boards, has been investigated in the past. The main causes of passive nonlinearities are usually associated with the contact effects, soldered joints, electro-thermal phenomena, ferroic materials and protective coatings.

Nonlinearities can be localised (e.g. due to contact effects) or distributed (e.g. due to nonlinear resistivity of signal tracks or substrate polarisability in printed circuits). Moreover, several commensurable sources of PIM generation may co-exist in one circuit. In this case, accurate identification of all physical sources is required for proper model retrieval.

In this paper, the mechanisms of PIM generations in printed transmission lines (TL) have been investigated experimentally and modelled using the formalism of X-parameters. The devised equivalent circuit models have been applied to the analysis of microstrip lines with distributed and cascaded lumped sources of nonlinearity. To assess the effect of printed TL layout on PIM generation rate, the dynamic PIM measurements have been carried in the straight and meandered microstrip lines. The paper is organised as follows. The experimental setup and test specimens are described in Section II. The effects of PIM generations in the microstrip TL with a single and pair of cascaded lumped nonlinearities are discussed in Section III. The X-parameter based model of distributed PIM generation in the TL is outlined in Section IV and a means of discriminating lumped and distributed PIM sources are discussed Section V. The results of dynamic measurements of PIM products in the straight and meandered microstrip TL are discussed in Section VI and the main findings are summarised in Conclusion.

II. EXPERIMENTAL SETUP

A commercial Rosenberger two-tone PIM analyser IM-209S [2] has been used for single port measurements of reverse PIM. The analyser calibration was verified with a standard −110 dBm EGSM PIM source. The residual level of the third-order PIM (PIM3) products in the test setup was measured at −120 dBm for 2×43 dBm carriers.

The PIM measurements were carried out at the input port of the transmission line under test terminated in a matching low-PIM load. The test setup was deployed in a screened anechoic chamber and special care was taken to protect the board surface and connectors from contamination by dust of Radar Absorbing

Material (RAM), which proved to have a strong impact on the PIM results. In some instances, the PIM analyser failed to display the actual PIM level, presumably due to the locked-in sources, so any abnormalities in PIM results were carefully assessed to eliminate the measurement artefacts.

Test specimens of microstrip lines were fabricated on a single panel of the TLG-30 board ($\varepsilon_r = 3.0$, $\tan\delta = 0.0026$, laminate thickness $h = 0.76$ mm and low-profile copper foil of thickness $t = 17.5$um) with the dominant substrate nonlinearity. The signal strips of width 1.9 mm provided the characteristic impedance of 50 Ω. The specimen set included:

- Two straight uniform lines of lengths 502 mm and 914 mm labelled "S502" and "S914", respectively
- Two meandered uniform lines of total lengths 1515 mm and 1955 mm labelled "M1515" and "M1955", respectively as shown in Fig. 1.

In order to investigate the effect of multiple PIM sources in printed circuits, the measurements have been carried out first with discrete sources of nonlinearities placed on the top of signal strips of the tested microstrip lines.

III. Cascaded Lumped Nonlinearities

PIM products generated by localised nonlinearities in microstrip lines form interference pattern which varies with the distance between the PIM sources. To illustrate this effect, lumped nonlinearities were emulated in the S914 line by placing pieces of paper with small pencil marks of size 2×2 mm^2 on top of the microstrip tracks. In a small signal regime, no discernible effect of such inclusions on the linear S-parameters was detected. However, when 2×43 dBm carriers of frequencies $f_1 = 935$ MHz and $f_2 = 960$ MHz were injected into the microstrip line, level of the reverse PIM3 products of frequency 910 MHz increased from −100 dBm in the original bare line to −63 dBm in the line with an artificial PIM source.

Then a pair of almost identical pencil marks spaced apart for Δl was placed on the strip conductor at distances $l_s = 30$ cm and $(l_s - \Delta l)$ from the input. The reverse PIM level versus variable spacing Δl between the pencil marks is shown in Fig. 2 at PIM3 frequency of 910 MHz. This plot demonstrates that maxima and minima of PIM3 level are offset for a quarter of the wavelength of PIM3 products in the microstrip line ($\lambda \approx 21.2$ cm at frequency of 910 MHz). This provides a clear evidence of the interference pattern of PIM3 products generated by the two lumped sources. It can also be observed that the peak level of the PIM3 in Fig. 2 is slightly lower as the second source is farther away from input, cf. PIM3 levels at $\Delta l = 20$ cm and $\Delta l = 10$ cm.

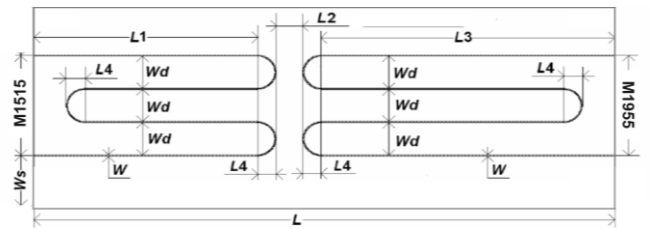

Fig. 1. Printed layout of the meandered lines with the dimensions in mm: L=914; W=1.9; Ws=87; Wd=85.1; $L1$=350; $L2$=42.6; $L3$=460; $L4$=29.9

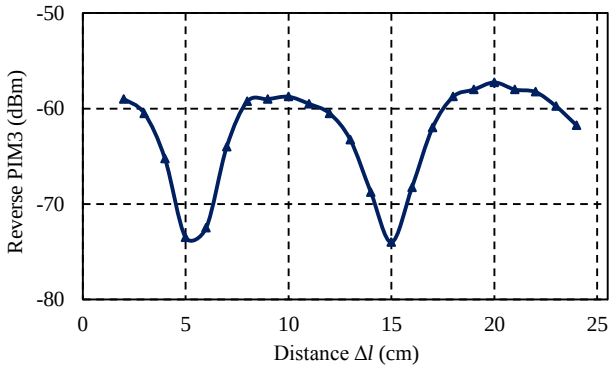

Fig. 2. Dependency of the reverse PIM3 products on the pencil mark location.

The interference patterns created by the artificial localised PIM sources can be instrumental for detecting lumped nonlinearities in distributed circuits, e.g. contact nonlinearity of launchers or soldered joints in antenna feed network. Indeed, if a lumped PIM source of magnitude commensurate with the PIM level in a test sample is placed on the top of signal strip and moved along the printed line under test, the resulting pattern of reverse PIM similar to that in Fig. 2 would imply the presence of internal localised PIM sources in the test line as further detailed in Section V. The concept of cascading closely spaced lumped nonlinearities can also be applied to modelling PIM in TL with distributed nonlinearities.

IV. Distributed PIM Generation

Weakly nonlinear distributed system can be described as cascaded circuits with lump nonlinearities. The X-parameters are particularly instrumental for this purpose [4], [5]. In order to apply the X-parameter formalism to the analysis of PIM generation by passive devices with distributed nonlinearities, the actual physical structure should be partitioned in a set of primitive constituent unit cells. Once an electrical size of the unit cell is much smaller than a wavelength, each cell can be described by a lumped element equivalent circuit. For example, linear *RLC* networks are often used for the analysis of the TLs, canonical discontinuities and their assemblies. Such models can be applied to the analysis of PIM generation in complex networks with multiple nonlinearities using the X-parameters. The required circuit characteristics of particular physical sources of nonlinearity can be retrieved from multi-parameter data fitting for the measured test standards.

Our equivalent circuit model of the nonlinear TL has been validated against the characteristic features of distributed PIM generation in the degenerative four-wave mixing, such as a cumulative growth of the forward PIM products towards the TL output and regular undulations of the reverse PIM level [3], [7] at the input. A section of uniform nonlinear microstrip line has been analysed using the Harmonic Balance solver in the Agilent ADS simulator. The TL has been partitioned in short segments, each described by an equivalent *RLC* circuit shown in Fig. 3. The nonlinear capacitor on the schematic represents a weak nonlinearity of the substrate.

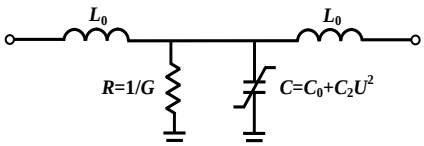

Fig. 3. Unit cell of nonlinear transmission line

The electrical length of each unit cell in Fig. 3, defined in terms of the phase shift, has been chosen at 2° that provides better than 20 dB return loss in the frequency range from DC to 3 GHz. The forward and reverse PIM3 products are generated by two CW tones of frequencies f_1 = 935 MHz and f_2 = 960 MHz with power levels of 44 dBm. To realise the 2° phase shift at PIM3 frequency $2f_1$-f_2 = 910 MHz the circuit elements had the following parameters: L_0 = 0.154 nH, $G = 3\times10^{-5}$ S, C_0 = 0.123 pF. The nonlinear capacitance $C_2 = 2.1\times10^{-11}$ pF/V^2 was chosen compatible with the experimental data reported in [3], [6], [7].

The calculated magnitudes of PIM3 products are shown in Fig. 4 in dependence of the electrical length θ of the nonlinear TL. Comparison of the simulated and measured forward PIM3 products in Fig. 4(a) demonstrates their very good correlation. Both curves exhibit similar rates of the cumulative growth of forward PIM3 products with the line length. The decaying periodic undulations of the reverse PIM3 level in Fig. 4(b) are in agreement with the analytical model of distributed PIM generation in [7].

The presented lumped element model of the TL with distributed nonlinearity is next applied to discrimination of lumped and distributed PIM sources in transmission lines.

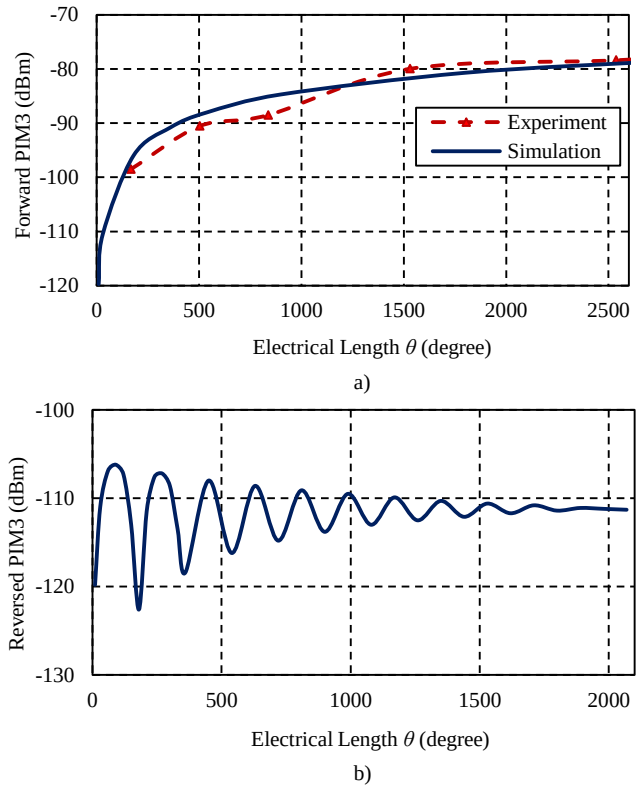

Fig. 4. Forward (a) and reversed (b) PIM3 products versus electrical length of the nonlinear transmission line.

V. Discrimination of the Lumped and Distributed Nonlinearities in Transmission Lines

The approach described in Section IV is equally applicable to modelling nonlinear TLs containing lumped nonlinearities. To this aim, let us consider a reference nonlinear transmission line of electrical length θ_2 = 900° described by the same model in Fig. 3. In the following simulations the nonlinear capacitance C_2 is presumed constant ($C_2 = 2.1\times10^{-14}$ pF/V^2).

A weak lumped nonlinearity is assumed in input microstrip launcher and it is represented by a nonlinear capacitor $C' = C_0' + C_2'U^2$ where $C_0' = 5.2\times10^{-3}$ pF is fixed and its value is chosen to limit variations of the small-signal S-parameters, i.e. the TL with the lumped nonlinearity remains matched. In practice, the value of C_2' is unknown a priory and in our experiment we have considered different scenarios by varying C_2' in the range from 0 to 9×10^{-9} pF/V^2.

Pencil mark is used as a probe nonlinearity to identify the mechanism of PIM generation in the test TL, i.e. discriminate distributed or localised sources. The convenience of the pencil mark as a PIM source is associated with the fact that it can be easily adjusted to produce the nonlinear response commensurate with the PIM level of the test specimen with combined distributed (fixed) and localised (launcher contact) nonlinearities. Besides, a pencil mark does not introduce any electrical discontinuity, so for ease of the analysis below we use the capacitor model of the pencil mark similar to that of the microstrip launcher but with a different value of the nonlinearity. The latter is chosen to provide ~ 5 dB higher forward PIM when we insert the pencil mark in the TL with a given launcher nonlinearity.

Once the pencil mark is moved along the transmission line and the reverse PIM3 level is recorded at each probe position at distance Δl (in degrees at 910 MHz) from input port. The simulated forward and reverse PIM3 magnitudes at frequency of 910 MHz (the carriers of 2×43 dBm power at frequencies f_1 = 935 MHz and f_2 = 960 MHz were applied) are shown in Fig. 5 in dependence of the pencil mark position.

The three curves in Fig. 5 correspond to different values of the launcher nonlinearity. The pencil mark nonlinearity in each case is chosen as described above. As one can observe, undulations of the reverse PIM3 level strongly depend on the strength of the launcher nonlinearity, relative to the distributed nonlinearity of the reference TL - the higher the launcher nonlinearity, the greater undulations. Moreover, the position of a lumped nonlinearity with reference to the TL input can also be located with the aid of the nonlinear probe, provided that the nonlinearity is strong enough.

VI. Dynamic Characteristics of PIM3 Products in Printed TL with Discontinuities

Dynamics of PIM generation, i.e. PIM product dependence on carrier power and frequency, usually provides a distinctive signature of the dominant source of nonlinearity. The PIM growth rate with carrier power is fundamentally related to the underlying physical mechanisms of PIM generation. Similarly, frequency sweep can identify particular types of nonlinearity.

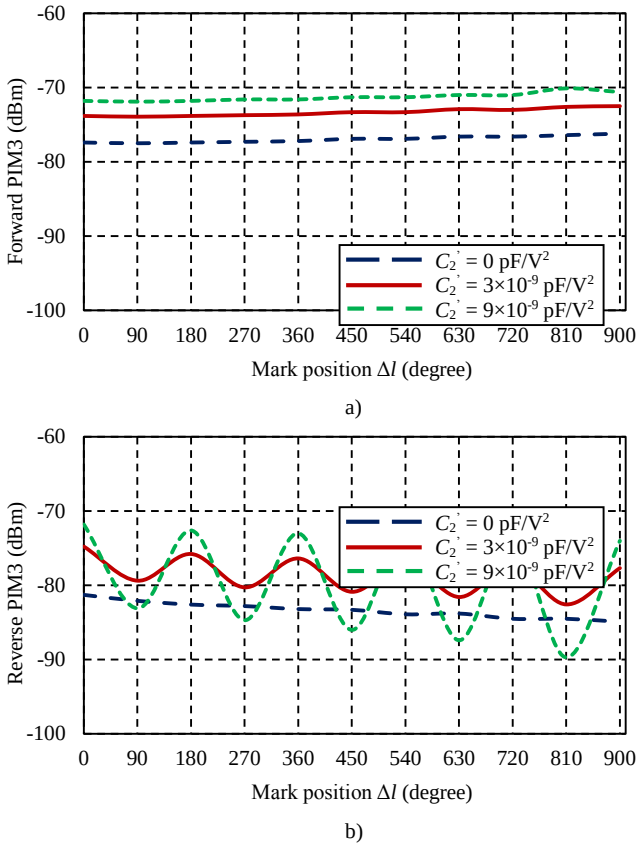

Fig. 5. Simulated forward (a) and reverse (b) PIM3 products versus pencil mark position.

The effect of carrier input power on PIM3 performance of straight and meandered microstrip lines has been investigated with the test specimens specified in Section II. Fig. 6 shows the reverse PIM3 magnitude versus carrier power for the 4 measured samples. It is noteworthy that at the carrier power in the range 36 - 46 dBm, PIM3 products generated in the measured microstrip lines are already close to saturation [3]. Therefore, the interpolated slope of the PIM3 in Fig. 6 is smaller than the classical 3:1, as earlier observed in [8]-[11].

However, the experimental curves in Fig. 6 exhibit a peculiar feature of intersection point at input carrier power of 36 dBm. In addition, the PIM3 slopes for the two meandered TL considerably differ from those for the straight TL. Our simulations with the basic polynomial models show that such behaviour cannot be explained by the effect of the line length only. On the other hand, it has been suggested elsewhere that the use of non-analytical polynomials can help reproduce the observed trends see, e.g., [11], **Error! Reference source not found.**. Nevertheless, the polynomial models of PIM generation still can be used, but they need further extension to include other mechanisms of nonlinearity and higher order approximations. Additional experimental studies are necessary to verify these conjectures and provide consistent and reliable experimental results.

To gain deeper insight in the dynamic characteristics of PIM generation, reverse PIM3 products have been measured in the sweep frequency mode at several fixed levels of carrier power.

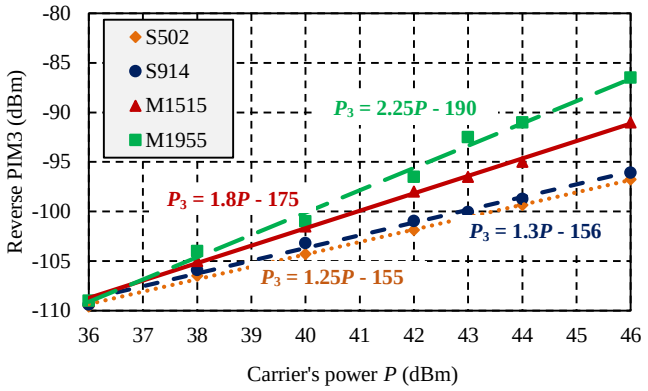

Fig. 6. Reverse PIM3 measurements at PIM3 frequency of 910 MHz vs. carrier's power. The carrier's power P represents the mean power of the two carriers. Straight lines P_3 are only eye guide to indicate the slope of PIM3 products for each test specimen.

Frequency of one carrier had been fixed at f_2 = 960 MHz whilst the other carrier frequency f_1 was swept in the range 925 – 937 MHz. The measurement results at PIM3 frequency $f_3 = 2f_1 - f_2$ are shown in Fig. 7 for both straight and meandered TL at variable carrier power.

Only minor variations of reverse PIM3 level across the measured frequency band are observed in Fig. 7, especially at lower power level of the carriers. This is conventionally interpreted as manifestation of memoryless nonlinearity. However, the effect of dynamic nonlinearities can be clearly observed at higher power of carriers. Moreover, the dynamics of PIM3 generation in the meandered TL distinctively differ from that in the straight TL. This indicates significant effect of the conductor layout on the interference patterns of the carriers and PIM3 products in the meandered lines, particularly near the strip bends. Also, cross-coupling between parallel sections of the meandered lines may alter reverse PIM3 response at input ports.

CONCLUSION AND DISCUSSIONS

Mechanisms of PIM generations in printed TL have been investigated experimentally and modelled using the formalism of X-parameters. The devised equivalent circuit models have been applied to the analysis of microstrip lines with distributed and cascaded lumped sources of nonlinearity. Microstrip TLs of different length and geometry were simulated and measured using a single-port PIM analyser. It has been shown that the line length and the presence of several cascaded lumped nonlinearities strongly influence the overall PIM level. It was also demonstrated that discontinuities can cause additional PIM products which alter the nonlinear response of the distributed circuit due to the interference with other sources. The measured reverse PIM3 products generated by cascaded nonlinearities in microstrip lines proved to be in full correlation with the simulations based upon the principles of phase synchronism. These results have provided explicit evidences that the distributed PIM generation in printed circuits fundamentally depends on the phase coherence of carriers and PIM products. Experimental demonstration of this effect has important

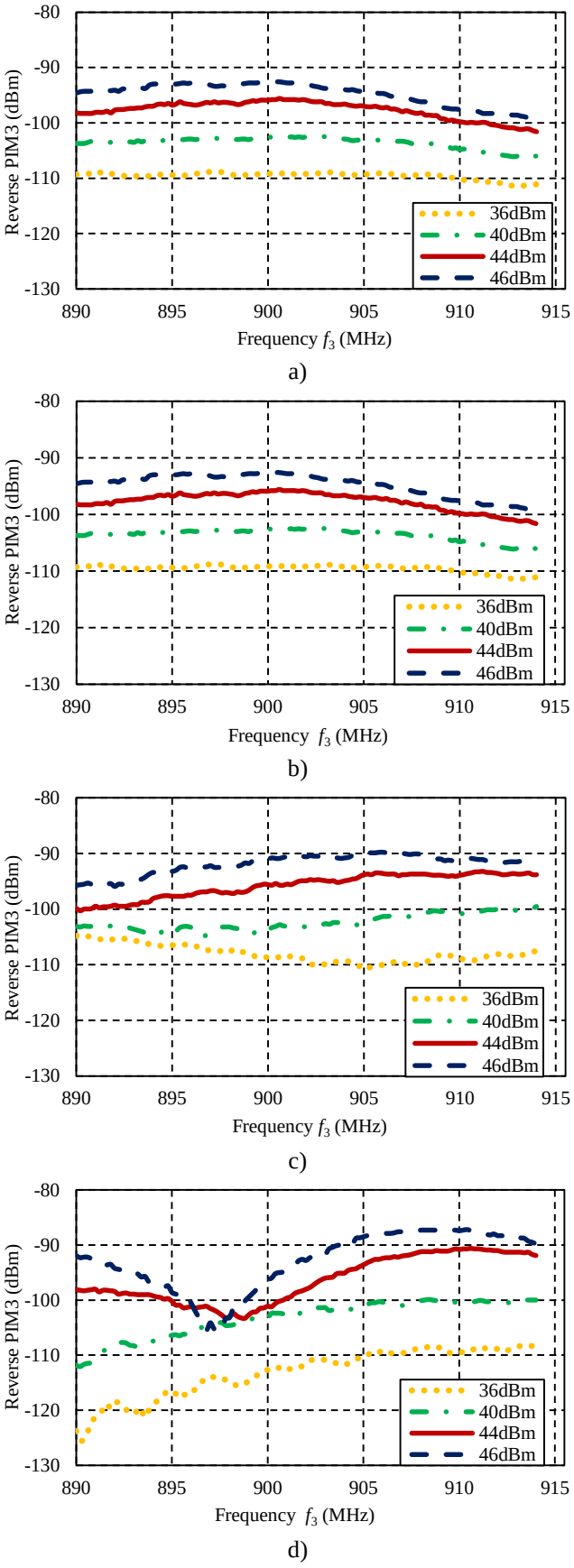

Fig. 7. Measured reverse PIM3 products versus swept frequency f_3 at carriers' power variable in the range 36 dBm – 46 dBm on the samples: a) S502, b) S914, c) M1515 and d) M1955.

implications for integrity of the phase modulated signals in base station antennas and RF front-end.

The dynamic PIM measurements have revealed that PIM3 generation rates in the straight and meandered microstrip lines differ and significantly deviate from those anticipated for the respective discrete sources of nonlinearity. These results indicate that multiple physical sources of nonlinearity contribute to PIM generation in printed circuits. Extensive experimental investigations are still necessary to identify and quantify the mechanisms of PIM generation in the microstrip lines with complex conductor layouts and combinations of the discrete and distributed nonlinearities. Further experiments are also necessary to explore the effects of localised discontinuities, PIM leakage and cross-coupling between the circuit elements in complex printed layouts.

ACKNOWLEDGEMENT

This work is supported by FP7 Marie Curie ITN ARTISAN, grant no. 316426. The authors would like to thank Mr David Bedford of Rosenberger Hochfrequenztechnik GmbH & Co. for providing the PIM analyser for this work.

REFERENCES

[1] P. L. Lui, "Passive intermodulation interference in communication systems", *Electron Electronics & Communication Engineering Journal*, Vol. 2, Issue 3, pp. 109-118, June 1990.

[2] http://www.rosenberger.com/en/products/communication/pim.php

[3] A. P. Shitvov, D. E. Zelenchuk, A. G. Schuchinsky, and V. F. Fusco, "Passive intermodulation generation on printed lines: near-field probing and observations," *IEEE Transactions on Microwave Theory and Techniques*, vol. 56, no. 12, Part 2, pp. 3121-3128, December 2008.

[4] J. Verspecht and D. Root, "Polyharmonic Distortion Modeling," IEEE Microwave Magazine, vol. 7, no. 3, pp. 44-57, June 2006.

[5] A.P. Shitvov, D.S. Kozlov and A.G. Schuchinsky, "Communication Nonlinearities Techniques for Analysis of Passive Intermodulation", 8-th International Workshop on Multipactor, Corona and Passive Intermodulation in Space RF Hardware, MULCOPIM' 2014, 17-19 September 2014, Valencia, Spain.

[6] M. Li, R. E. Amaya, R. G. Harrison and N. G. Tarr, "X-Parameter Measurement of Pulse-Compression Nonlinear Transmission Lines," *Journal of Electrical and Computer Engineering*, vol. 2010.

[7] D. E. Zelenchuk, A. P. Shitvov, A. G. Schuchinsky, and V. F. Fusco, "Passive intermodulation in finite lengths of printed microstrip lines," *IEEE Transactions on Microwave Theory and Techniques*, vol. 56, no. 11, Part 1, pp. 2426-2434, November 2008.

[8] A. P. Shitvov, D. E. Zelenchuk, A. G. Schuchinsky "Carrier-Power Dependence of Passive Intermodulation Products in Printed Lines", in *Proc. LAPC 2009*, 16-17 Nov., 2009, Loughborough University, UK, pp. 177-180.

[9] J.R. Wilkerson, K.G. Gard, A.G. Schuchinsky, M.B. Steer, "Electro-Thermal Theory of Intermodulation Distortion in Lossy Microwave Components", *IEEE Trans. on Microwave Theory and Techniques*, vol. 56, no. 12, Part 1, pp. 2717-2725, Dec. 2008.

[10] J. R. Wilkerson, P. G. Lam, K. G. Gard, and M. B. Steer, "Distributed passive intermodulation distortion on transmission lines," *IEEE Trans. Microwave Theory & Tech.*, vol. 59, no. 5, pp. 1190-1205, May 2011.

[11] A. Shitvov, A.G. Schuchinsky, M.B. Steer, J.M. Wetherington, "Characterisation of nonlinear distortion and intermodulation in passive devices and antennas," *8th European Conf. on Antennas and Propag. EuCAP*, pp.1454-1458, 6-11 April 2014.

[12] J. Sombrin, G. Soubercaze-Pun, I. Albert, "Relaxation of the multicarrier passive intermodulation specifications of antennas," *8th European Conf. on Antennas and Propag. EuCAP*, pp.1647-1650, 6-11 April 2014.